Available online at www.sciencedirect.com
SCIENCE DIRECT®
Journal of Hydrology 321 (2006) 59–76
Journal of Hydrology
www.elsevier.com/locate/jhydrol

Modeling width adjustment in meandering channels

D. Chen*, J.G. Duan[1]

Division of Hydrologic Science, Desert Research Institute, 755 E. Flamingo Road, Las Vegas, NV 89119, USA

Received 1 November 2004; revised 30 March 2005; accepted 11 July 2005

Abstract

Widening in sinuous channels occurs when the retreat of the outer bank exceeds the advance of the opposite bank. An analytical model is presented to simulate width adjustment in meandering channels of non-cohesive bank material resulting from bank erosion of two interactive processes: basal erosion and bank collapse. Bank collapse refers to the avalanche of non-cohesive material in the upper part of bank above water surface resulting from over-steepening of the bank surface due to basal erosion. The rate of basal erosion, including lateral erosion and bed degradation, is calculated as a function of the longitudinal gradient of sediment transport rate and strength of secondary flow. The transverse bed slope is treated as a variable that increases as channel sinuosity increases until the transverse bed slope reaches its maximum value. By simplifying the bank-collapse process for non-cohesive materials, the present study shows that the rate of bank-line retreat is determined by lateral erosion rate, near-bank bed-degradation rate, sediment grain size, and difference between flow depth and bank height. The time-dependent widening processes of two meandering channels in the laboratory are selected to test applicability of the model. The result shows that the simulated bank lines at individual time intervals closely match the experimental measurements. Whether the sinuosity of a meandering channel will increase or decrease is primarily determined by didtribution of the lngitudinal gradient of sediment transport rate along the channel.

Keywords: Width adjustment; Bank erosion; Meander; Sediment transport; Analytical model

1. Introduction

Channel widening, as a result of bank erosion, attracts substantial attention from engineers and scientists because the retreat of bank lines can seriously affect floodplain dwellers, damage riparian vegetation, and endanger bridge crossings and bank-protection structures (ASCE TC, 1998). Eroded, fine-grained bank material may pose a hazard to aquatic habitats and contribute to sedimentation problems downstream (Darby and Thorne, 1994). However, width adjustment, especially in meandering channels, is a complex morpho-dynamic process resulting from the interactions between flow, sediment, and movable boundaries. These adjustments can be triggered by either climate change or anthropogenic activities, such as urban growth or stream realignment. Therefore, modeling width adjustment is still a challenging

* Corresponding author. Tel.: +1 702 862 5541; fax: +1 702 862 5427.
E-mail addresses: dchen@dri.edu (D. Chen), gduan@dri.edu (J.G. Duan).
[1] Tel.: +1 702 862 5452; fax: +1 702 862 5427.

0022-1694/$ - see front matter © 2005 Elsevier B.V. All rights reserved.
doi:10.1016/j.jhydrol.2005.07.034

problem in the area of river engineering despite the importance of understanding width-adjustment process.

Studies of channel width adjustment can be divided into two approaches according to respective objectives: one approach is to predict the equilibrium channel under regime conditions (stable, long-term) and the other approach is to simulate the processes underlying meander evolution. Empirical regime formulas developed from field observations and regression analyses have been used to correlate the geometry of equilibrium channels with basin characteristics, such as drainage areas (Dunne and Leopold, 1978; Montgomery and Gran, 2001), bankfull or effective discharge (Leopold and Maddock, 1953; Hey and Thorne, 1986; Kellerhals and Church, 1989; Knighton, 1998), and sediment grain size (Schumm, 1968; Ferguson, 1973). The empirical equations have been successfully applied to predict regime conditions of alluvial channels.

Extremal theories assume that alluvial channels attain equilibrium when an indicator (e.g. stream power, rate of energy dissipation, concentration of suspended sediment, etc.) reaches its maximum or minimum (ASCE TC, 1998). These theories include the minimum stream power (Yang, 1976; Chang, 1979), maximum sediment transport efficiency (Kirkby, 1977) or capacity (White et al., 1982; Millar and Quick, 1993; 1998), minimum variance (Williams, 1978), and the principle of least action (Huang and Nanson, 2000; Eaton et al., 2004). The width of the equilibrium channel was also determined using the threshold concept of sediment incipient motion (Glover and Florey, 1951; Lane, 1955) or, more realistically, by accounting for the lateral diffusion of downstream momentum (Parker, 1978; Ikeda et al., 1988; Ikeda and Izumi, 1990, 1991; Kovacs and Parker, 1994; Vigilar and Diplas, 1997).

In general, extremal theories lack physical foundation and are used infrequently to model the width-adjustment process, which often is of greater interest than the shape of the equilibrium channels (Sun et al., 1996). Osman and Thorne (1988) developed a process-based model to predict channel-width adjustment by accounting for the combined effects of lateral erosion and mass instability in producing bank instability. This method was modified by Darby and Thorne (1994); Darby and Thorne (1996), and Simon et al. (2000) to predict the width and volume of mass failure. However, it is difficult to use this method to predict bank failure without a precise prediction of basal erosion. Ikeda et al. (1981) assumed the rate of bank erosion is linearly related to the magnitude of near-bank velocity perturbation, a difference between depth-averaged velocity and cross-sectional mean velocity. This assumption was employed in numerous subsequent studies (Parker et al., 1982; 1983; Parker, 1983;Parker and Andrew, 1986; Johannesson, 1985; Johannesson and Parker, 1989; Odgaard, 1989; Larsen, 1995; StØlum, 1998; Sun et al., 1996, 2001a,b). The Ikeda et al., 1981 model directly correlated the rate of bank erosion with the near-bank flow field, however, this assumption could be unrealistic because bank retreats and advances depend on whether sediment is accumulated or washed away from bank toe where the near-bank excessive velocity could be less or greater than zero.

In recent years, numerical models emerged as a cost-effective tool to simulate the morpho-dynamic process of alluvial channels. Increasingly, two- and three-dimensional computational hydrodynamic (CFD) models are applied to simulate the morpho-dynamic processes of meandering streams (Mosselman, 1998; Nagata et al., 2000; Duan et al., 2001; Darby et al., 2002; Olsen, 2003). Mosselman (1998); Nagata et al. (2000); Duan et al. (2001), and Darby et al. (2002) coupled process-based bank erosion models with two-dimensional, depth-averaged models of flow and bed topography in movable computational grids. Duan et al. (2001) indicated that the rate of bank retreat or advance depends on the longitudinal gradient of sediment transport, strength of secondary flow, and erosion of sediment from the bank. Darby et al. (2002) considered the deposition of failed bank material at the toe of the bank and its subsequent removal. However, Mosselman (1998); Darby et al. (2002) calculated basal erosion through a method similar to the simple assumption set forth by Ikeda et al. (1981). In addition, Mosselman (1998); Duan et al. (2001) neglected the bank-failure process, whereas Nagata et al. (2000) neglected the difference between basal erosion and bed degradation. As we will discuss in the following paragraphs, higher and steeper banks are more likely to collapse than lower and less steep banks; therefore, the bank height above

the water and critical side slope should be considered when the bank erosion rate is calculated.

In the present study, the bank erosion model of Duan et al. (2001) is modified by extending the control volume to half of the channel width and taking accounting for the effects of bed-degradation and bank-collapse processes. Bank collapse in this paper, as cited in Nagata et al. (2000), refers to the avalanche of non-cohesive material in the upper part of bank above water surface resulting from over-steepening of the bank surface due to basal erosion. To test the applicability of the modified model, the present study implements an analytical flow model and simulates the widening processes of two meandering channels in a laboratory.

The two-dimensional flow field in a sine-generated channel was solved using the linear theory (Johannesson and Parker, 1989). Concerning the phenomenon of bank erosion for non-cohesive material, two consequent basal erosion and bank collapse, were recognized. The rate of basal erosion is determined primarily by the gradient of sediment transport rate in the longitudinal direction, while previous research indicated the rate of basal erosion was proportional to the magnitude of excessive near-bank velocity or shear stress. The present study assumes channel banks are composed of non-cohesive materials so that the rate of bank-line retreat is a function of the rate of basal erosion (including lateral erosion and bed-degradation), bank material grain size, and difference between flow depth and bank height. The current model is limited to non-cohesive bank material. When applied to natural rivers, more realistic bank failure models for cohesive and stratified bank material must be developed.

2. Model development

2.1. Flow model

The flow-governing equations are two-dimensional, depth-averaged, steady-flow, Reynolds-averaged Navier–Stocks equations in channel-fitted, curvilinear, orthogonal coordinates written as follows

$$\frac{\partial(hu)}{\partial s} + \frac{\partial}{\partial n}[(1 + nC)hv] = 0 \tag{1}$$

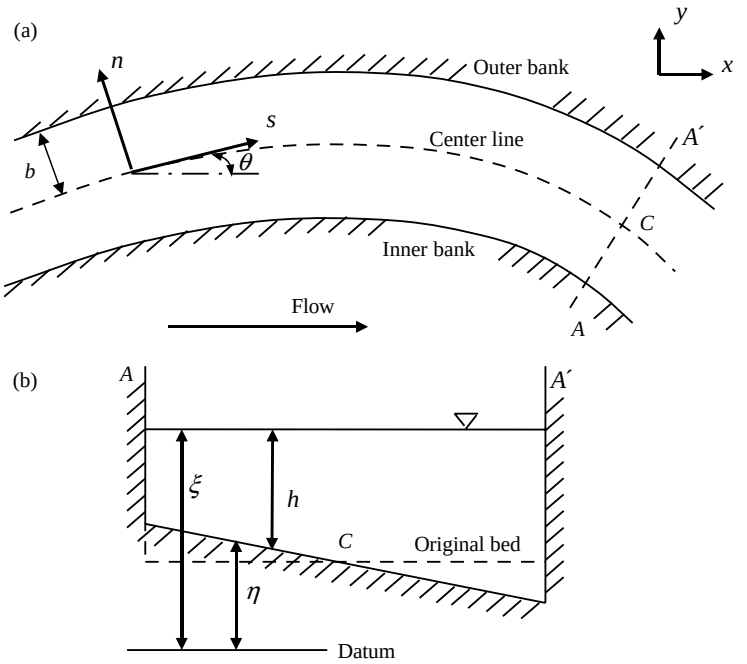

Fig. 1. Definition of variables and coordinate system: (a) plain view; (b) channel cross-section.

$$\frac{1}{1+nC}u\frac{\partial u}{\partial s}+v\frac{\partial u}{\partial n}+\frac{C}{1+nC}uv = \frac{-1}{1+nC}g\frac{\partial \xi}{\partial s}-C_{\mathrm{f}}u\frac{(u^2+v^2)^{1/2}}{h} -\frac{1}{h}\left[\frac{\partial}{\partial n}\left(uh\int_{\eta}^{\xi}Tv_{\mathrm{s}}\,\mathrm{d}z\right)+\frac{2C}{1+nC}uh\int_{\eta}^{\xi}Tv_{\mathrm{s}}\,\mathrm{d}z\right] \quad (2)$$

$$\frac{1}{1+nC}u\frac{\partial v}{\partial s}+v\frac{\partial v}{\partial n}-\frac{C}{1+nC}u^2=-g\frac{\partial \xi}{\partial n}-\frac{\tau_{\mathrm{n}}}{\rho h} \quad (3)$$

where u and v denote depth-averaged velocity components in the longitudinal and transverse directions, respectively; z axis is aimed upward; g is the acceleration of gravity; ξ and η denote water surface and bed elevation, respectively; ρ is water density; h is flow depth; and C is the curvature of the channel centerline defined as follows

$$C(s)=\frac{\mathrm{d}\theta}{\mathrm{d}s}=\frac{1}{r} \quad (4)$$

where θ is the deflection angle between the down-channel direction and the x axis, and r is the local radius of curvature. Fig. 1 gives the coordinate system and physical definitions of the variables.

The two integral terms on the right-side of Eq. (2) are dispersion terms resulting from the redistribution of streamwise momentum due to secondary flow (Johannesson and Parker, 1989). T is a dimensionless shape function describing the vertical variation of streamwise velocity having a depth-averaged value of unity, and v_{s} is secondary flow velocity in the transverse direction.

The planform of natural meandering channels can be approximated simply by sine-generated curves (Langbein and Leopold, 1966). The periodic shape of a meandering loop is depicted by the angle of the channel centerline (θ) with respect to the down-valley direction and wavelength of the meandering loop. The mathematical expression for the sine-generated curve can be written as follows

$$\theta=\theta_0\cos(ks) \quad (5)$$

where K is dimensionless wave number given by $k=bk$ and $k=2\pi/\lambda$; b is half-width of channel; λ is the meander wavelength; and θ_0 is the value of θ at the deflection point of two consecutive meandering loops. Assuming the ratios of flow depth and channel width to the radius of channel curvature are small and neglecting the second-order terms in Eqs. (1)–(3), the first-order solution of streamwise velocity, including the effect of dispersion terms for sine-generated meandering channels, is obtained as

$$u=U+UNbk\theta_0[-\alpha\cos(ks)+\beta\sin(ks)] \quad (6)$$

where U is the reach-averaged primary velocity, and b is the normal half-width of the channel. The value of N ranges from a negative unity at the inner bank to a positive unity at the outer bank. The parameters α and β can be expressed as follows

$$\alpha=\frac{kHC_{\mathrm{f}}(A+A_{\mathrm{s}}+F^2+1)}{H^2k^2+4C_{\mathrm{f}}^2} \quad (7)$$

$$\beta=\frac{2C_{\mathrm{f}}^2(A+A_{\mathrm{s}}+F^2-1)-H^2k^2}{H^2k^2+4C_{\mathrm{f}}^2} \quad (8)$$

where C_{f} is the Chezy friction coefficient; F is the Froude number defined as $F=U/\sqrt{gH}$; H is the reach-averaged flow depth; A is the scour factor, which characterizes the transverse bed slope; and A_{s} represents the momentum redistribution effect exerted by the secondary current. Similar solutions were derived by Johannesson (1985); Johannesson and Parker (1989) where the dispersion terms were found to be essential in distributing flow momentum. Smith and Mclean (1984); Nelson and Smith (1989), and Blanckaert and de Vriend (2003) stressed the non-linearities in flow hydrodynamics. As channel curvature and bar amplitude increase, non-linearity in the flow solution can be expected to play an increasing role in the flow dynamics and thus influence the shape and evolution of meandering channels.

The second-order solution including both non-linearities and dispersion terms (Imran et al., 1999) proved to be effective when applied to a submarine meandering modeling. However, researches (Ikeda et al., 1981; Parker et al., 1982; Parker, 1983; Parker and Andrew, 1986) have shown that a linear solution is sufficient in simulating flow and the evolution of the meandering process when channel curvature is mild or moderate. In reality, the intensity of flow and

sediment transport tends to subside as the meander evolves due to the increased length of the channel and gentler slope. Let channel sinuosity be defined as $\delta = \Lambda/\lambda$, where Λ is the meander length along centerline (m); λ is the meander wavelength (m). A meandering channel is considered mildly curved when $\delta < 1.2$, moderately curved when $1.2 < \delta < 1.5$, and highly curved when $\delta > 1.5$ (Rosgen, 1996) The findings of Julien (2002) indicate the migration rate of meanders is at a maximum when sinuosity is approximately 1.34. This evidence also agrees with the observations of Friedkin (1945); Schumm et al. (1987), and Hickin and Nanson (1975) analysis of field data, which showed that the rate of channel migration reaches its maximum at relative curvature $R/B = 2$–3, where R is the radius of centerline curvature (m); B is the channel width (m). According to the relation between channel sinuosity and relative curvature given by Langbein and Leopold (1966), $R/B = 2$–3 is equivalent to $\delta = 1.1$–1.4. The objective of the present study is to use experimental laboratory cases ($\delta \approx 1.07$) to verify a newly developed bank erosion model that indicates the reasonableness in physical process by relating bank erosion to the gradient rather than the excess or deficit of streamwise velocity. The solution to the flow hydrodynamic field expressed in Eq. (6) is accurate for the purposes of the present study.

In Eq. (6), parameter A_s represents the strength of the secondary current, and parameter A quantifies the transverse bed slope. The linear expression of A (Johannesson and Parker, 1989) is shown below:

$$\frac{\partial \eta}{\partial n} = -AHC \tag{9}$$

At the apex of a sine-generated meandering channel where $ks = \pi/2$, Eq. (7) gives

$$u = U$$

$$\frac{u-U}{U} = UNbk\theta_0 \left[\frac{2C_f^2(A + A_s + F^2 - 1) - H^2k^2}{H^2k^2 + 4C_f^2} \right] \tag{10}$$

The parameter A vanishes when the channel bed is flat in the transverse direction (Johannesson and Parker, 1989). The parameter A_s can be neglected in mildly sinuous channels ($\delta < 1.2$) when the secondary flow is weak. The flow in natural rivers is most likely to be subcritical with the Froude number being less than unity. Therefore, the denominator in the parenthesis is positive for subcritical flow, and $u > U$ is valid near the inner bank when $-1 \le N < 0$, regardless of sinuosity and wavelength. This conclusion agrees with the experimental results of Chang (1971); Silva (1995); Shiono and Muto (1998), which showed that the locus of high velocities remained close to the inner banks of a flat-bed, sine-generated channel until reaching a downstream inflection point. On the other hand, a number of laboratory experiments (Friedkin, 1945; Hickin, 1972; Schumm et al. (1987)) proved that a highly-sinuous natural channel can be developed from a straight or low-sinuous flat-bed channel by eroding the outer bank. This means that retreat of banklines does not occur at the high-velocity zone. Rather, the bank erosion model of Duan (1998); Duan et al. (2001) showed that the advance or retreat of bank lines related directly to the gradient of streamwise velocity. Although the maximum streamwise velocity exists at the inner bank of the apex when channel have no transverse slope, the maximum acceleration of streamwise velocity occurs at the downstream apex where the bank erodes. The longitudinal distribution of gradient of streamwise velocity results in the downstream migration as well as lateral extension and downstream rotation of meandering loops.

The center streamline of the channel is defined to distinguish flow acceleration and deceleration zones. The gradient of longitudinal velocity and rate of sediment transport can also be calculated by using the center streamline. The channel centerline divides the cross-section of a meander into two equal parts, one on the left and one on the right, whereas the center streamline separates flow discharge into two equal parts at each cross-section. These two lines are the same in a straight channel. However, they differ from each other in a meandering channel because flow velocity is distributed non-uniformally along the transverse. When the center streamline deviates from the channel centerline toward the outer bank, the gradient of longitudinal velocity and rate of sediment transport are positive because the flow converges.

The mathematical expression for center streamline was obtained by integrating Eq. (6) to satisfy the

following equation

$$\int_{-b}^{Y} u\,\mathrm{d}N = \frac{1}{2}\int_{-b}^{b} u\,\mathrm{d}N \tag{11}$$

where Y represents the transverse coordinate of the center streamline, and u is the streamwise velocity expressed in Eq. (6). The solution to Eq. (11) yields

$$Y = \frac{\sqrt{1 + b^2k^2\theta_0^2[-\alpha\cos(ks) + \beta\sin(ks)]^2 - 1}}{k\theta_0[-\alpha\cos(ks) + \beta\sin(ks)]} \tag{12}$$

Y denotes the transverse coordinate of the center streamline ranging from $-b$ to b. When $Y=-b$, the center streamline is located at the left bank; when $Y=0$, the center streamline is located at the center of the channel; and when $Y=+b$, the center streamline is located at the right bank.

2.2. Bank erosion model

Bank erosion of non-cohesive material consists of two interactive physical processes: basal erosion and bank collapse (Nagata et al., 2000). Basal erosion refers to the fluvial entrainment of bank material by flow-induced forces acting on the bank surface-drag force, resistance force, and lift force. Basal erosion does not guarantee retreat of the bank line because the collapsed bank material may be deposited at near banks, such as sand bars, and thus cause the bank line to advance. The rate of bank erosion traditionally is calculated empirically from the geometry of channel bends, bank material, and flow intensity (Hickin, 1977; Hooke, 1980). Process-based bend migration models (Johannesson, 1985; Odgaard, 1989; Sun et al., 2001a,b) successfully extended the Ikeda et al. (1981) bank erosion theory to model long-term trends of meandering evolution in complex sedimentary environments. These models represent the authentic assumption that the rate of bank erosion is proportional to the excess near-bank velocity; however, this assumption could be unrealistic because the advance and retreat of bank lines are determined by sediment mass balance near banks. Duan et al. (2001) solved the two-dimensional, depth-averaged momentum and continuity equations expressed in Cartesian coordinates for the flow field. Although sediment transport and lateral bank erosion were considered, bed degradation and geotechnical bank failure or collapse was neglected in Duan et al. (2001). In the present study, the Duan et al. (2001) bank erosion model was modified by extending the control volume to half of channel width b and accounting for the effect of bed-degradation and bank-collapse processes. The modified bank erosion model, derived from the mass conservation law for near-bank cells, was employed to simulate the migration of bank lines. The simulated initiation, migration, and evolution of a meander indicated that the rate of bank erosion is a function of the longitudinal gradient in sediment transport, strength of secondary flow, and mass wasting from bank collapse.

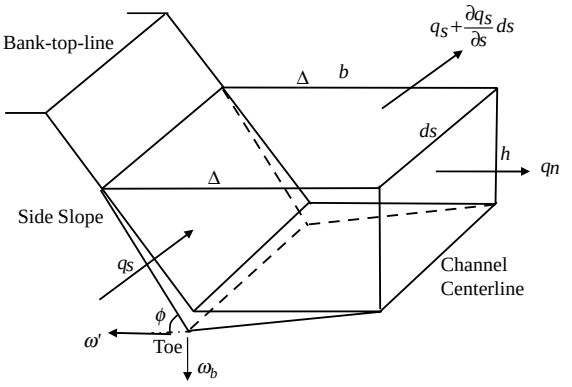

Fig. 2. Sediment flux balance in half of a cross-section.

2.2.1. Advance and retreat of bank-lines

Bank erosion eventually causes banks to advance or retreat. Bank advancement is caused by the deposition of sediment near the bank. This sediment can come from an eroded bank or bed material transported from upstream. Banks retreat as they are eroded, and the material is transported away by the flow. Predicting bank advance or retreat is based on a balance (or mass conservation) of the sediment in a control volume near the bank, including sediment from bank erosion and bank failure or collapse, sediment stored on the bed due to deposition, and sediment fluxes transported in and out of the control volume. Fig. 2 illustrates bank geometry and sediment flux balance in the control volume. Initially the transverse slope of the channel is zero, and the angle of the bank surface is equal to the angle of repose for

non-cohesive bank material. The sediment continuity equation can be written as follows

$$\left(q_s + \frac{\partial q_s}{\partial s}\,\mathrm{d}s\right)b - q_s b + q_n\,\mathrm{d}s = -\omega' \frac{h\,\mathrm{d}s}{2}(1-P)\rho_s - \omega_b \frac{b\,\mathrm{d}s}{2}(1-P)\rho_s \quad (13)$$

where ω' is the lateral bank erosion rate defined as the distance of bank retreat at the bank toe per unit of time in the transverse direction; ω_b denotes the bed-degradation rate at the bank toe; ρ_s is the sediment density; q_s and q_n are the component sediment transport rates per unit width in the s and n directions, respectively; and P is porosity.

Rearranging Eq. (13) produces

$$\omega' = -\omega_b \frac{b}{h} - \frac{2}{h\rho_s(1-P)}\left(\frac{\partial q_s}{\partial s}b + q_n\right) \quad (14)$$

River bank material is often different from bed material (Darby and Thorne, 1994); therefore, ω' is not necessarily equal to ω_b. Eq. (14) indicates that the rate of lateral erosion can be estimated by the rate of bed degradation, longitudinal gradient of sediment transport rate, transverse sediment transport rate, and channel geometry (i.e. b, h). However, the actual distance of bank retreat, as observed and measured in the field, is the distance that the top bank line retreats per unit time rather than the distance of basal erosion per unit time occurring under the water surface. The rate of bank erosion is derived as the distance of bank retreat or advance occurring at the top bank lines. Fig. 3 schematizes bank erosion processes including bed degradation, lateral erosion, and bank collapse. In Fig. 3, the dashed line [line (1)] represents the initial bed and bank surfaces, and line (1) changes to the dash-dot line [line (2)] after bed degradation and lateral erosion occurs. Banks having slopes that are greater than the angle of repose are unstable; therefore, the line (2) is transient, and the collapsed bank material from the upper bank (the area of ECBI) will deposit immediately at the bank toe (fill the area of IFG) to form a bank surface of the same repose angle. Therefore, the solid line [line (3)] shows the cross-sectional profile after bank collapse occurs. Fig. 3 shows that the distance of lateral migration (symbolized as ΔL) and bed degradation (symbolized as ΔZ) occurring during a short time step, ΔT, will result in the collapse of upper bank materials; consequently, the bank line retreats (symbolized as ΔB). Hasegawa (1981) proposed a similar model that was successfully applied by Nagata et al. (2000) in simulating laboratory experiments of meandering evolution. The mass volumes per unit length depicted in the area of ECBI and IFG are equal, and the areas of triangle BFH and parallelogram EDHC are equal as well according to Nagata et al. (2000). The following mathematical expression is produced

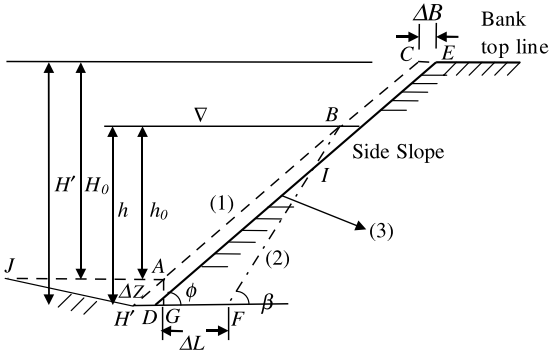

Fig. 3. Sediment flux balance in half of a cross-section.

$$\frac{1}{2}(\Delta L + \Delta Z\cot\phi)(h_0 + \Delta Z) = \Delta B(H_0 + \Delta Z) \quad (15)$$

where h_0 and H_0 are initial near-bank flow depth and bank height, respectively, and ϕ is the angle of repose. Therefore, the distance of bank retreat can be calculated from Eq. (15) and expressed as follows

$$\Delta B = \frac{(\Delta L + \Delta Z\cot\phi)(h_0 + \Delta Z)}{2(H_0 + \Delta Z)} = \frac{(\Delta L + \Delta Z\cot\phi)h}{2H'} \quad (16)$$

where H' is the bank height after basal erosion occurs. Dividing ΔT at both sides of Eq. (16) yields

$$\frac{\Delta B}{\Delta T} = \frac{h}{2H'}\left(\frac{\Delta L}{\Delta T} + \frac{\Delta Z}{\Delta T}\cot\phi\right) \quad (17)$$

By applying the definitions for the rate of bank retreat, bed degradation, and lateral erosion, Eq. (17) becomes

$$\omega = \frac{h}{2H'}(\omega' + \omega_b\cot\phi) \quad (18)$$

where $\omega = \lim_{\Delta T \to 0} (\Delta B/\Delta T)$ represents the retreat rate of the bank top line. By substituting Eq. (14) into Eq. (18), the following expression results:

$$\omega = \omega_b \frac{h \cot \phi - b}{2H'} - \frac{1}{(1-P)\rho_s H'} \left(\frac{\partial q_s}{\partial s} b + q_n \right) \quad (19)$$

Eq. (19) indicates that the retreat rate of the bank top line can be calculated by using the rate of bed degradation; longitudinal gradient of the sediment transport rate; transverse sediment transport rate; properties of bank materials such as the angle of repose and porosity; flow parameters (i.e. b, h); and bank geometry (e.g. bank height, etc.). The calculation of sediment transport rates (q_s, q_n) in Eq. (19) is discussed in Section 2.2.

From Eq. (9), one can obtain the following expression:

$$\eta|_{n=b} = -bAHC \quad (20)$$

Therefore, the rate of bed degradation at the toe of the outer bank can be expressed as

$$\omega_b = \frac{\partial \eta}{\partial t}\bigg|_{n=b} = -\frac{\partial (b\, AHC)}{\partial t} \quad (21)$$

H remains constant throughout. Therefore, the following expression results:

$$\omega_b = -bHA \frac{\partial C}{\partial t} - bHC \frac{\partial A}{\partial t} \quad (22)$$

Eq. (22) is valid when the channel curvature is mild. In Eq. (22), $\partial C/\partial t$ is calculated at each time step for individual channel planform. The term,$\partial A/\partial t$, is discussed in Section 3. The parameter A ranged from 0 to A_{max}, corresponding to the process where the transverse bed slope developed from zero to its maximum value. The analytical expression for the maximum value of A is discussed in Section 4.1.

2.2.2. Empirical sediment transport equations

Eq. (19) requires a formula to calculate the streamwise sediment transport rate, and for the present study, the Leiwei bed-load equation (Chien et al., 1989) was selected. This formula is valid for a wide range of sediment particle grain sizes ($D = 0.25$–23 mm) and flow conditions ($H/D = 5$–500). The Leiwei bed-load equation is expressed as follows:

$$q_s = 2D \left(\frac{U}{\sqrt{gH}} \right)^3 (U - U_c) \left(\frac{D}{H} \right)^{1/4} \quad (23)$$

where D is the mean grain size of sediment particles, and U_c is the reach-averaged incipient velocity for bed load. Eq. (23) is rewritten as follows

$$q_s = k_q U^4 \quad (24)$$

where $k_q = 2D^{1.25}/(g^{1.5}H^{1.75})$, and $U \geq U_c$ is assumed.

The first-order derivative of q_s in the longitudinal direction is obtained through the following expression:

$$\frac{\partial q_s}{\partial s} = k_q 4U^3 \frac{\partial U}{\partial s} \quad (25)$$

Ikeda (1989) derived the transverse bed-load transport rate by analyzing the force balance of a moving spherical particle on a plane inclined in both longitudinal and transverse directions. The ratio of transverse and longitudinal bed load transport rate was derived as

$$C_s = \frac{q_n}{q_s} = \tan \varphi + \frac{1 + \frac{C_L}{C_D}\mu}{\chi \mu} \sqrt{\frac{\tau_C}{\tau}} \tan \psi \quad (26)$$

where C_s is the ratio of q_n to q_s; ϕ is the angle where the bed-shear stress deviates from the s direction; $\tan \psi$ is the transverse bed slope, whose maximum can be calculated by formulas found in the literature (Kikkawa et al., 1976; Ikeda, 1989); μ is the coefficient of the kinetic friction between the particles and equals 0.43 (Kikkawa et al., 1976; Ikeda, 1989); χ is the ratio of the kinetic friction coefficient to the static friction coefficient, which equals 0.59 (Ikeda, 1989);τ_C and τ are the critical and actual bed shear stresses, respectively; and C_D and C_L are the drag and lift coefficients, respectively. Concerning a spherical sand particle placed on a rough bed, Kikkawa et al. (1976) suggested that $C_L/C_D = 0.85$ and $C_D = 0.4$. Engelund (1974) derived the direction of the resulting bed-shear stress expressed with the deviation angle written as $\tan \phi = (\tau_n/\tau_s) = 7.0h/r$. Eq. (26) represents the correlation between bed-load transport rates in the s and n directions. Then, the transverse bed-load transport rate can be obtained with the following expression:

$$q_n = C_s k_q U^4 \tag{27}$$

Eq. (27) is used to calculate bed-load transport rate in the transverse direction. The coefficient C_s can be determined using Eq. (26).

2.2.3. Maximum value of A for equilibrium cross-sections

As discussed in the preceding paragraphs, the parameter A quantifying the transverse bed slope vanishes when the channel bed is flat at its beginning. As the meandering planform evolves, the transverse bed slope develops until reaching its maximum value. Other studies (Engelund, 1974; Kikkawa et al., 1976; Zimmerman and Kennedy, 1978; Ikeda et al., 1981; Parker and Andrew, 1986; Odgaard, 1989) have been conducted where a constant value for A was assumed, which implicitly assumed the existence of a transverse bed slope at the beginning of meandering development (Engelund, 1974; Kikkawa et al., 1976; Zimmerman and Kennedy, 1978; Ikeda et al., 1981; Parker and Andrew, 1986; Odgaard, 1989). In the present study, the parameter A ranged from 0 to A_{max}. An equation expressing the maximum value of A can be derived by using the Kikkawa et al. (1976) relation for an equilibrium transverse slope written as follows

$$\frac{\partial \eta}{\partial n} = -\left(\frac{3}{4}\frac{\mu C_D}{1+\mu\frac{C_L}{C_D}}\right)^{1/2} \frac{v_b}{\left[\left(\frac{\rho_s}{\rho}-1\right)gD\right]^{1/2}} \tag{28}$$

where μ is the coefficient of kinetic friction between sediment particle and bed; C_D and C_L are drag and lift coefficients, respectively; and ρ_s and ρ are sediment and water densities, respectively. Let v_b and u_b denote the components of near-bed velocity in the n and s directions, respectively, Engelund (1974) obtained the following correlation:

$$v_b = 7.0\frac{h}{r}u_b \tag{29}$$

The velocity distribution satisfies the exponential law

$$u_b = (1+m)\left[\frac{(D/2)}{h}\right]^m U \tag{30}$$

where $m = 1/6$–$1/7$. Replacing the near-bed velocity, u_b, with Eq. (30), Eq. (28) then becomes

$$\frac{\partial \eta}{\partial n} = -\left(\frac{3}{4}\frac{\mu C_D}{1+\mu\frac{C_L}{C_D}}\right)^{1/2} \frac{7.0HC'}{\left[\left(\frac{\rho_s}{\rho}-1\right)gD\right]^{1/2}}(1+m)\left(\frac{D}{2H}\right)^m U \tag{31}$$

For quasi-uniform flow, the local flow depth h is replaced by the reach-averaged flow depth, H, in Eq. (31). Combining Eq. (31) with Eq. (9), the mathematical expression for A in the equilibrium cross-section is derived as follows:

$$A_{max} = \left(\frac{3}{4}\frac{\mu C_D}{1+\mu\frac{C_L}{C_D}}\right)^{1/2} \frac{7.0}{\left[\left(\frac{\rho_s}{\rho}-1\right)gD\right]^{1/2}}(1+m)\left(\frac{D}{2H}\right)^m U \tag{32}$$

Eq. (32) shows that the maximum value of A for the equilibrium cross-section is determined by flow depth, velocity, lift and drag coefficients, friction coefficient, and particle grain size of bed material.

2.2.4. Rate of channel-width adjustment

Narrowing in sinuous channels occurs when the rate of alternate or point bar growth exceeds the rate of retreat of the cut bank opposite. Conversely, widening in sinuous channels may occur when outer bank retreat, due to toe scouring, exceeds the rate of advance of the opposite bank, due to alternate or point bar growth (Nanson and Hickin, 1983; Pizzuto, 1994; ASCE TC, 1998). Schumm (1985) and Simon and Thorne (1996) state that the process whereby stability is recovered is characterized by aggradation of the channel bed and fluvial deposition on the banks. Schumm (1985) refers to the bank-deposition feature as berms. Bank failure or collapse is commonly caused by geotechnical instability of bank and may dominate the bank erosion process resulting in, for example, incised channels. In the present study, the fundamental mechanism in bank collapse is destabilization in the upper part of the bank due to basal erosion occurring at the bank toes. Advance or retreat of bank lines is determined by combining Eqs. (19), (22), (25), and (27):

$$\omega = b\left(-HA\frac{\partial C}{\partial t} - HC\frac{\partial A}{\partial t}\right)\frac{h\cot\phi - b}{2H'} - \frac{1}{(1-P)\rho_s H'}\left(4k_q bU^3\frac{\partial U}{\partial s} + C_s k_q U^4\right) \quad (33)$$

Applying Eq. (33) at the left bank for the left half of the cross-section yields:

$$\omega_1 = b\left(-HA\frac{\partial C}{\partial t} - HC\frac{\partial A}{\partial t}\right)\frac{h_1\cot\phi - b}{2H'} - \frac{1}{(1-P)\rho_s H'}\left(4k_q bU_1^3\frac{\partial U_1}{\partial s} + C_s k_q U_1^4\right) \quad (34)$$

Similarly, applying Eq. (33) at the right bank for the right half of the cross-section yields,

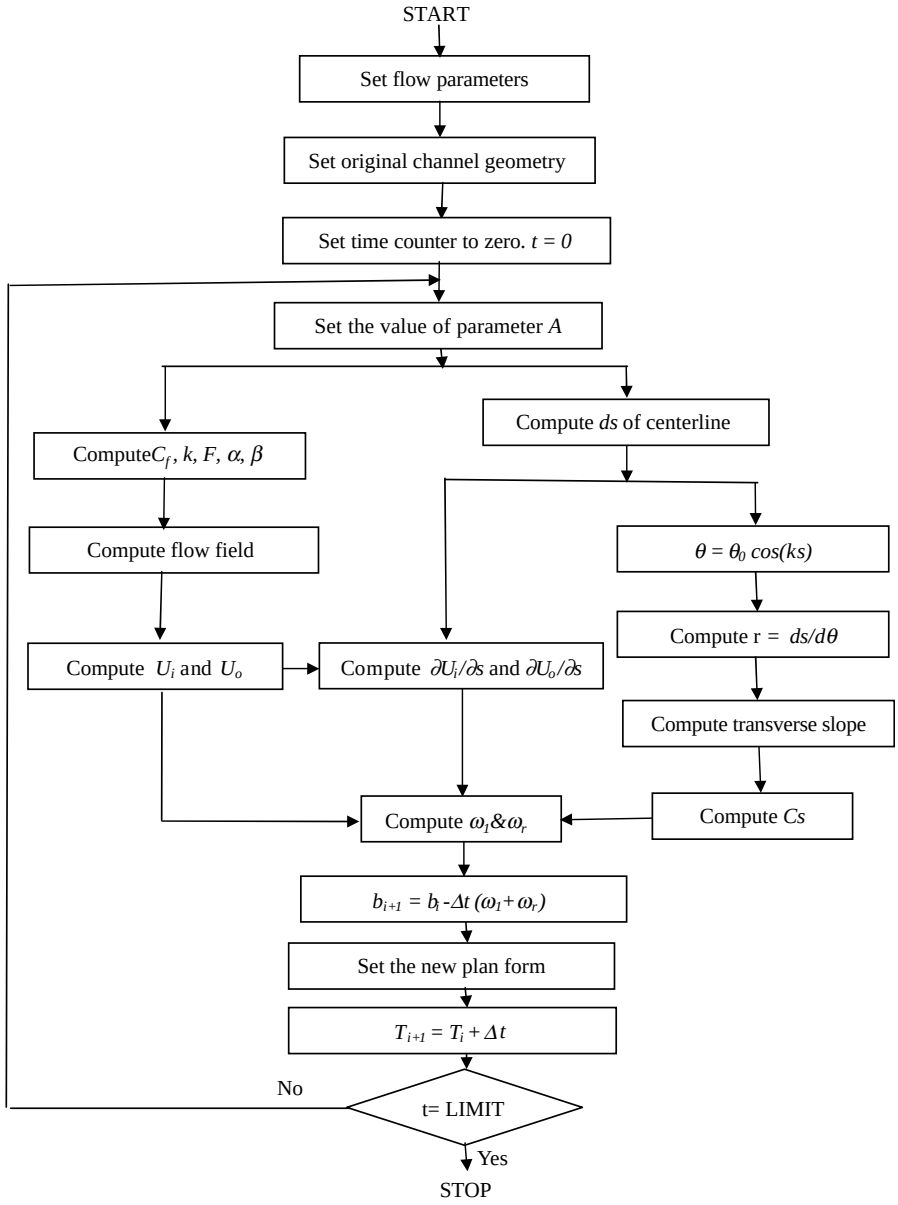

Fig. 4. Program flowchart.

$$\omega_r = b\left(-HA\frac{\partial C}{\partial t} - HC\frac{\partial A}{\partial t}\right)\frac{h_r \cot\phi - b}{2H'} - \frac{1}{(1-P)\rho_s H'}\left(4k_q b U_r^3 \frac{\partial U_r}{\partial s} + C_s k_q U_r^4\right) \quad (35)$$

The subscript 'l' and 'r' denote variables for the left and right banks, respectively.

The channel width b_i adjusted to b_{i+1} at the next time step $i+1$ is written as:

$$b_{i+1} = b_i - \Delta t(\omega_l + \omega_r) \quad (36)$$

If the flow regime and sediment supply are quasi-steady over periods of decades or centuries, the morphology of the river adjusts to create a metastable, equilibrium channel width (ASCE TC, 1998). The outer bank retreats at the same rate as the opposite bank advances (i.e. $\omega_l = -\omega_r$), and the channel then maintains a constant width as its planform evolves. This assumption of constant width was employed by the model of Ikeda et al. (1981). Many natural rivers, however, cannot be considered to have equilibrium channels (ASCE TC, 1998). These rivers display significant morphological changes, including width adjustments as observed both in the laboratory (Nagata et al., 2000) and in the field (Nanson and Hickin, 1983; Pizzuto, 1994).

3. Numerical method

The finite difference method was used to discretize Eq. (36). Fig. 4 contains a flowchart depicting the operational protocol of the computer program. In the first step in the program, initial flow parameters, including U, H, J, and initial channel geometry, are set. The present model is applicable to a sine-generated channel where the planform is expressed by Eq. (5). Cross-sections are assumed to be trapezoidal in shape and the bank slope is set to equal to the angle of repose. The initial channel width, bank height, sediment particle size, and transverse bed slope are given at $t=0$. First-order derivatives of scalar variables, with respect to the s coordinate, are approximated by the central difference scheme.

$$\frac{d\Phi}{ds} \approx \frac{\Delta\Phi}{\Delta s} = \frac{\Phi_{i+1} - \Phi_{i-1}}{2\Delta s} \quad (37)$$

where Φ is a scalar variable.

The channel curvature, C, is calculated using Eq. (4). The parameter A is assumed to be a time-dependent variable as discussed in Section 3. The location of center streamline Y and the parameter C_s are calculated by using Eqs. (12) and (26), respectively. Once the difference between the center streamline and channel centerline is determined, U_l and U_r at each cross-section can be obtained. Their first-order derivatives, with respect to the s coordinate, can also be obtained using Eq. (37).

At the beginning of the computation, Eqs. (34) and (35) are used to calculate the distance of bank retreat at both banks. At the next time step, flow depth and velocity are solved by using the channel width and transverse bed slope from the previous time step. The transverse bed slope varies from zero to its maximum value at equilibrium. Then, the channel planform and curvature at the new time step are calculated using the newly obtained channel centerline, whose migration rate was obtained as follows:

$$2\omega = (\omega_l - \omega_r) \quad (38)$$

where ω is the rate of centerline migration.

4. Sensitivity analysis and model verification

4.1. Sensitivity analysis of A distribution function

Nagata et al. (2000) conducted four sets of experiments to study channel-width adjustment in meandering and straight channels. One set of these experiments (Run 2) was selected in the paper to determine the appropriate distribution function of parameter 'A'. The experimental results of Run 1 were chosen to verify the applicability of the developed model to simulate the widening processes of a sine-generated channel. The flume is 10 m long and 1 m wide with a depth of 0.2 m. A trapezoidal cross-section, with a bottom width of 14 cm, top width of 30 cm, and bank height of 4 cm, was formed at the beginning of both experiments. The bank and bed material in both experiments consisted of fairly uniform sand having a particle mean diameter of

1.42 mm, and the angle of repose was 34.3°. The initial planforms for both experiments were set as a sine-generated channel having a wavelength of 2 m and an initial angle $\theta_0 = 30°$. During both experiments, sediment was fed manually into the entrance of the channel. Temporal changes in bank lines were recorded by taking photographs, and bed profiles were measured using a point gauge and a laser bed profiler.

For the experiment Run 1, a constant discharge of 1.98 l/s was maintained at the inlet of the flume channel, which had a mean flow depth of 3.00 cm and a valley slope of 1/300. Bank boundary lines were measured at 15, 60, and 125 min during the experiment. The Chezy friction coefficient, C_f, was calculated by using Manning's equation and equaled 0.082. The parameter A_{max} equaled 2.02 when calculated using Eq. (32). The constant discharge at the inlet of Run 2 was 0.63 l/s, which was less than one-third of the discharge in Run 1. The flume channel had a mean flow depth of 1.5 cm and a valley slope of 1/100. Bank boundary lines were measured at 15, 60, and 120 min. The Chezy friction coefficient C_f was calculated as 0.220 by using Manning's equation. The parameter, A_{max}, in Run 2 equaled to 2.09 when calculated using Eq. (32).

Besides the calculation of A_{max} in the model, this section discusses the sensitivity analysis of modeling results to the selection of the A distribution function. Undoubtedly, along with the development of the transverse bed slope from zero to its maximum value in the experiments, the parameter A-adopted in the model-ranged from 0 to A_{max}. In experimental Run 2, for example, the value of A changed from 0 to 2.09 within 120 min; $A = A_{max}$ at 120 min when the transverse bed slope reached its maximum value in the experiments. However, it is not known how the value of A varies with time. In the present study, four functions were assumed in order to study how the value of A varies with time. These functions include assuming (a) A has a constant value of 2.00, (b) A varies linearly with time (Eq. (39)), (c) A varies as a Type I parabolic function of time (Eq. (40)), and (d) A varies as a Type II parabolic of time (Eq. (41)). The four time-dependent distribution functions are plotted in Fig. 5. For the linear distribution, the functional relation of A is written as:

$$A = \frac{t}{60} \tag{39}$$

The parabolic distribution of Type I is assumed to follow Eq. (40).

$$A = \sqrt{\frac{t}{30}} \tag{40}$$

The parabolic distribution of Type II is assumed to be:

$$A = \frac{t^2}{7200} \tag{41}$$

T ranges from 0 to 120 min for all the equations from (39) to (41) in Run 2.

Fig. 6 compares the influence of the four time-dependent distribution functions on parameter A, while the channel undergoes width adjustment in Run 2. In Fig. 6, the discrete rectangular points represent the data measured after 120 min in Run 2. The dashed line denotes the calculated planform after

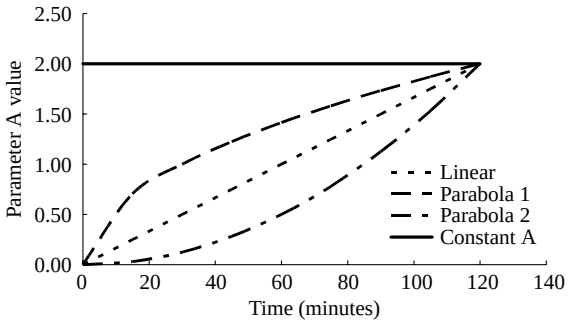

Fig. 5. Assuming the parameter A as different time variables.

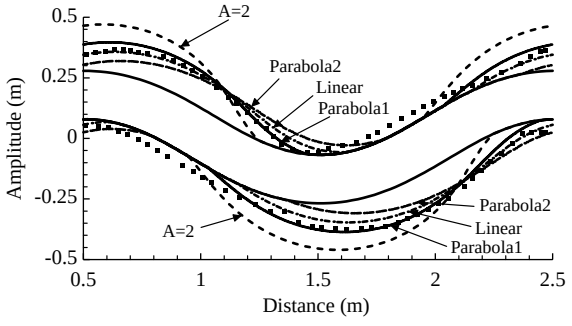

Fig. 6. Sensitivity analysis of various distribution functions for A (rectangular dots denote the measured boundary at $T = 120$ min in Run 2).

120 min using a constant, $A=2.00$. The dash-dot line denotes the calculated planform assuming a linear distribution of A (Eq. (39)). The dotted line denotes the calculated planform by assuming Type I parabolic distribution of A (Eq. (40)). The double-dot-dash line denotes the calculated planform by assuming Type II parabolic distribution of A (Eq. (41)). The results revealed that the channel migrated downstream too rapidly when the parameter A were defined by Eq. (39) or Eq. (41) but too slowly when A was assumed to be a constant. These scenarios are not realistic for natural rivers. The Type I parabolic distribution expressed in Eq. (40) yields the best result and was adopted in the following calculations.

4.2. Verification by experimental datasets

Run 1 was selected in the present study to verify applicability of the model to simulate the widening processes of meandering channel. During the experiment, constant flow was released at the inlet of an open-channel flume. The original channel has a sine-generated planform. The parameter A used in both experiments was assumed to be a time-dependent variable that satisfied the Eq. (40). In both experiments, the time step for flow computation, Δt, equaled 1/60 min, and grid size Δs equaled one-hundredth of the wavelength, λ. Flow parameters used in the simulations of both experiments are summarized in Table 1.

Banks advance with the development of point bars, while banks retreat when they are eroded and the eroded material is transported downstream. Point bars did not undergo detailed measurement in these experiments. Therefore, to be consistent in establishing experimental conditions, when the rate of bank retreat, as calculated with Eq. (33), was greater than zero (bank advance), the bank is assumed to be unchanged in the simulations. If the rate of bank erosion was less than zero, bank-lines were relocated.

Simulation results are summarized in Figs. 7–12 where flow direction is from left to right in all figures. Temporal changes in planforms for Runs 1 and 2 are plotted in Figs. 7 and 8, respectively. Simulated bank lines are compared with measured bank lines, and good agreement was observed at individual time intervals. As pointed out by Nagata et al. (2000), the channel tended to decrease its sinuosity in Run 1; however, the channel tended to develop in Run 2. To explain the two resulting types of channel processes that occurred in Runs 1 and 2, the center streamlines and longitudinal gradients of the sediment transport rates near the left banks are plotted in Figs. 9 and 10 at $t=0$. From Figs. 9 and 10, one can see that the center streamlines were deflected toward the inner banks at $t=0$ in both experiments, which means the higher-flow velocity zones existed adjacent to the inner banks in both cases. It is clear that erosion of the concave banks was not caused primarily by higher-velocity flows but rather by the higher-longitudinal gradients of sediment transport rates, as described in Section 2.2. Figs. 9 and 10 also plotted the longitudinal gradient of sediment transport rate near the left banks of both experiments, whose amplitudes and distributions along the channel matched the amplitudes and distributions of planform change. From Figs. 7 to 10, one can see that the highest degree of bank erosion and highest gradient of sediment transport rate occurred near the inflection points in Run 1, whereas they occurred downstream near the apexes in Run 2. Therefore, whether the sinuosity of a meandering channel will increase or decrease is primarily determined by distribution of the longitudinal gradient of the sediment transport rate along the channel.

Temporal changes in longitudinal distribution of the transverse bed slope in Run 2 are plotted in Fig. 11. Eq. (9) is used to calculate the transverse bed slope, and Fig. 11 verifies the applicability of Eq. (40). As shown in Fig. 11, the transverse bed slope at each cross-section increased with time, but the rate of

Table 1
Experimental flow conditions and parameters used in calculating the first time step

Run no.	Q (cm^3/s)	B (m)	J (m/m)	H (cm)	U (cm/s)	K	A_{max}	F	C_f	α	β
1	1980	0.14	1/300	3.0	23.5	0.41	2.02	0.43	0.082	0.21	−0.92
2	630	0.10	1/100	1.5	21.00	0.29	2.09	0.55	0.220	0.30	−0.55

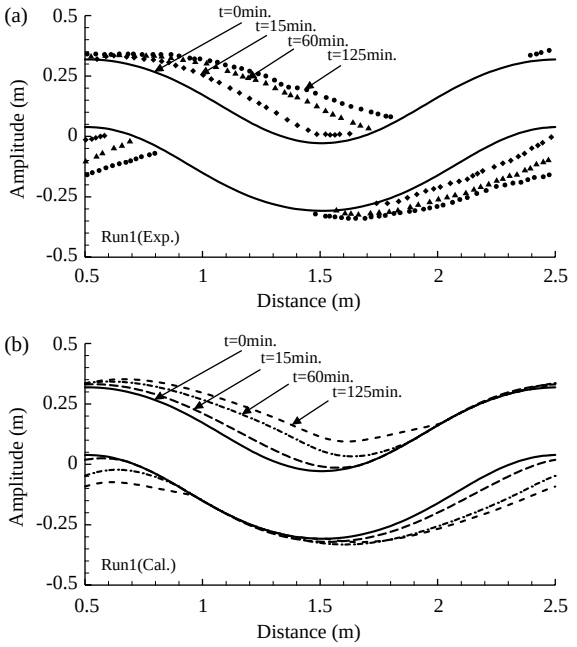

Fig. 7. Temporal changes in planforms (Run 1): (a) experimental data; (b) calculated data.

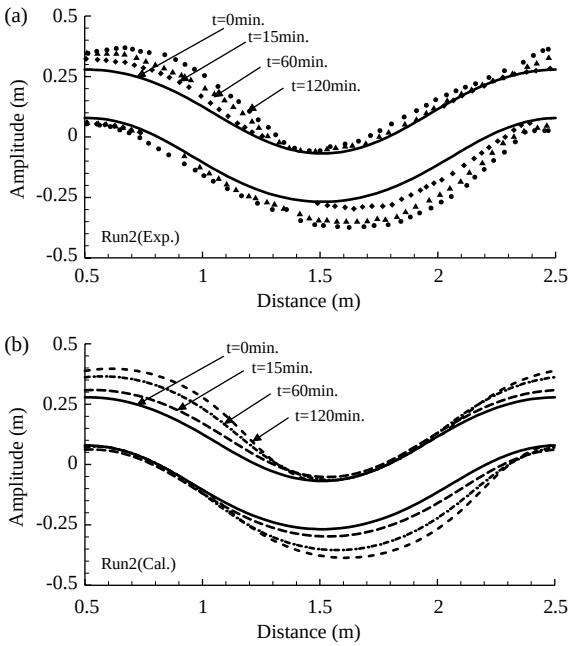

Fig. 8. Temporal changes in planforms (Run 2): (a) experimental data; (b) calculated data.

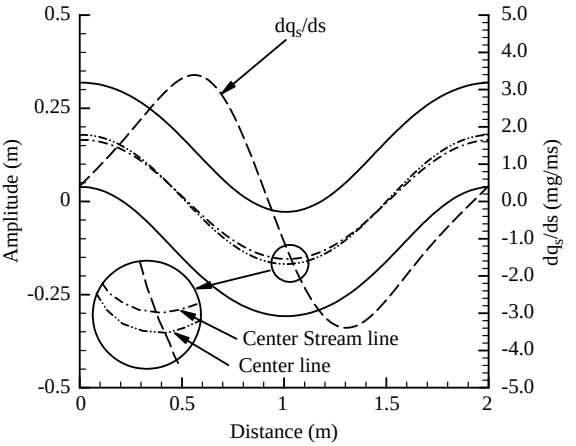

Fig. 9. Simulated results: center streamline and longitudinal gradient of sediment transport rate near the left bank at $t=0$ (Run 1).

increase was reduced over time. At each time interval, the maximum transverse bed slope occurred around the apexes. Temporal changes in the longitudinal distribution of local channel curvature are plotted in Fig. 12. The local curvature was derived from the new channel centerlines occurring at each time interval, and migration rates of the new channel centerlines are expressed with Eq. (38). The maximum channel curvature located the apexes, and the zero curvature located the inflection points. Fig. 12 indicates that the inflection points migrated downstream as the channel developed, but the apexes migrated first downstream

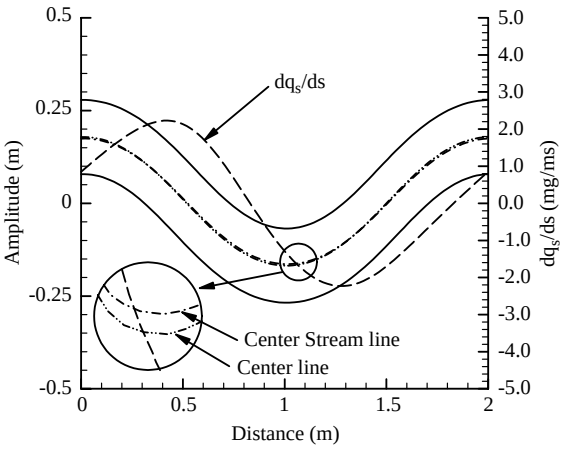

Fig. 10. Simulated results: center streamline and longitudinal gradient of sediment transport rate near the left bank at $t=0$ (Run 2).

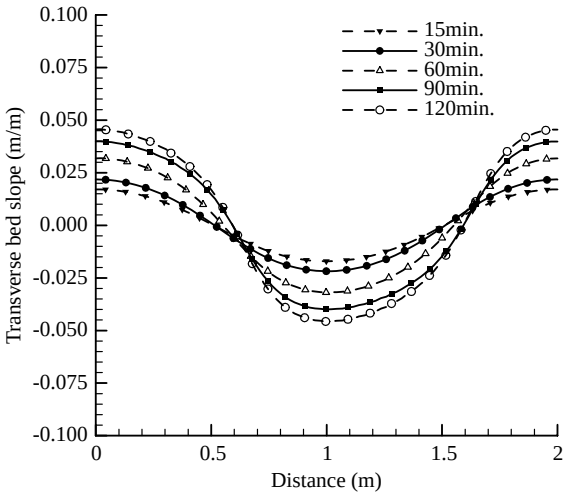

Fig. 11. Simulated results: Longitudinal distribution of transverse bed slope (Run 2).

and then upstream when the channel curvature became higher. The apexes migrated in this manner because the highest degree of bank erosion generally occurs somewhere downstream from the apex; however, the apex migrates upstream when the curvature becomes higher. Development of both the transverse bed slope and channel planform results from of the interaction between channel flow and boundaries, which inversely affect the forthcoming flow and sediment-transport fields. Therefore, it is important for a width adjustment model to calculate both flow and sediment–transport processes.

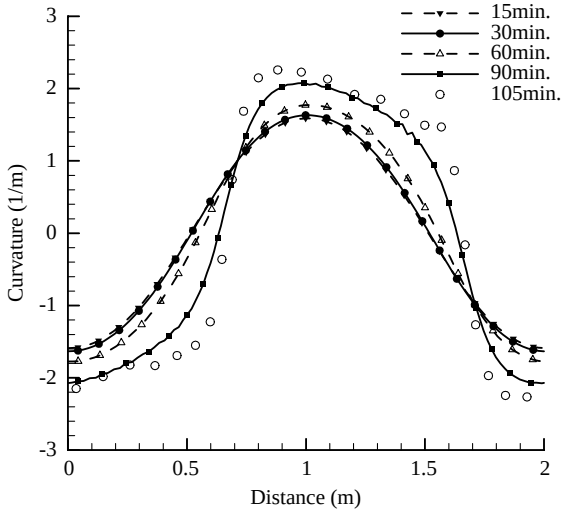

Fig. 12. Simulated results: Longitudinal distribution of the local channel curvature (Run 2).

5. Conclusions

The analytical model described for the present study was used to predict the time behavior of width adjustment in meandering channels. Special features of the model include (a) regarding the phenomenon of bank erosion for non-cohesive material, two consequent processes—basal bank erosion and bank collapse—were recognized; (b) the bank erosion model by Duan et al. (2001) was modified by extending the control volume to half-channel width and by accounting for bed-degradation and bank-collapse processes; and (c) the transverse bed slope was treated as a variable increasing with channel sinuosity until reaching its maximum value.

The following conclusions can be drawn from the present study.

(A) The rate that non-cohesive materials retreat at the top line of the bank was determined by the rate of lateral erosion; rate of near-bank bed-degradation; grain size of sediment particles; and difference between flow depth and bank height.

(B) The rate of basal erosion, including lateral erosion and bed degradation, is a function of the longitudinal gradient of sediment transport rate and strength of secondary flow rather than being proportional to the magnitude of excessive near-bank velocity or shear stress.

(C) It is more adaptive to treat the parameter A as a time variable rather than a constant. In the present study, a parabolic time–distribution of A value was selected, and calculated results matched the experimental data well under varying hydraulic conditions.

(D) Whether the sinuosity of a meandering channel will increase or decrease is primarily determined by distribution of the longitudinal gradient of sediment transport rate along the channel.

(E) The inflection points migrated downstream as the channel developed, but the apexes first migrated downstream and then migrated upstream when the channel curvature became higher.

In summary, the developed analytical model reasonably simulated the evolution processes of meandering channels. Natural rivers often have a stratified bank surface, and bank material is non-uniform. Further model development will consider multiple-grain-sized sediment, multi-layered bank surfaces, and deposition of debris and its subsequent removal from the bank toe.

Acknowledgements

This research project was sponsored by the US Department of Defense, Army Research Office (ARO), under Grant Number DAAD19-00-1-0157. The authors are very grateful for funding provided by ARO and for support provided by engineers involved in the project.

Notation

A scour factor, which characterizes the transverse bed slope
A_s parameter that represents the momentum redistribution effect exerted by the secondary current
b width of control volume (in the transverse direction) (m)
B width of channel (m)
C curvature of the channel centerline (m^{-1})
C_f Chezy friction coefficient
C_s ratio of q_n to q_s
C_d drag coefficient
C_L lift coefficient
D mean grain size of sediment particles (m)
d_s length of the control volume (in the streamwise direction) (m)
ΔB distance of bank retreat (m)
ΔL distance of lateral erosion at bank toe (m)
ΔZ distance of bed degradation (m)
ΔT time interval (s)
F Froude number
g gravitational acceleration (m/s^2)
h_0 initial near-bank flow depth (m)
h flow depth (m)
H' bank height (m)
H reach-averaged flow depth (m)
H_0 initial bank height (m)
k wave number (m)
δ channel sinuosity
Λ meander length along centerline (m)
λ meander wavelength (m)
n transverse coordinates (as a subscript)
N parameter that ranges from a negative unity at the inner bank to a positive unity at the outer bank
P porosity of sediment
q_s component volumetric bed load flux per unit width in the s direction (m^2/s)
q_n component volumetric bed load flux per unit width in the n directions (m^2/s)
r local radius of curvature (m)
R radius of centerline curvature (m)
s longitudinal coordinates
t time variation (s)
μ coefficient of the kinetic friction between particle and bed
ρ density of flow (kg/m^3)
ρ_s density of sediment (kg/m^3)
τ_s component flow shear stress in the s direction (N/m_2)
τ_n component flow shear stress in the n direction (N/m_2)
u depth-averaged velocity components in the longitudinal directions (m/s)
U reach-averaged velocity (m/s)
v depth-averaged velocity components in the transverse directions (m/s)
ϕ angle of repose (rad)
ξ water surface elevation (m)
η bed elevation (m)
θ_0 value of θ at the deflection point of two consecutive meandering loops (rad)
θ deflection angle between the down-channel direction and the x-axis (rad)
ω bank retreat rate (m/s)
ω' lateral erosion rate at bank toe (m/s)
ω_b bed degradation rate at bank toe (m/s)
χ ratio of kinetic friction coefficient to static friction coefficient

References

ASCE Task Committee, 1998. River width adjustment. I. Process and mechanisms. J. Hydraul. Eng., ASCE 9, 881–902.

Blanckaert, K., de Vriend, H.J., 2003. Nonlinear modeling of mean flow redistribution in curved open channels. Water Resour. Res. 39 (12), 6.1–6.14.

Chang, Y.C., 1971. Lateral mixing in meandering channels, PhD Dissertation, University of Iowa, Iowa City, IA.

Chang, H.H., 1979. Minimum stream power and river channel patterns. J. Hydrol. 41, 301–327.

Chien, N., Zhang, R., Chou, Z.D., 1989. River Evolution. Chinese Scientific Press, Beijing, China (in Chinese).

Darby, S.E., Thorne, C.R., 1994. Prediction of tension crack location and river bank erosion hazards along destabilized channels. Earth Surf. Proc. Land. 19, 233–245.

Darby, S.E., Thorne, C.R., 1996. Development and testing of riverbank-stability analysis. J. Hydraul. Eng. 122 (8), 443–454.

Darby, S.E., Alabyan, A.M., Van de Wiel, M.J., 2002. Numerical simulation of bank erosion and channel migration in meandering rivers. Water Resour. Res. 38 (9), 2.1–2.12.

Duan, G.H., 1998. Simulation of alluvial channel migration processes with a two-dimensional numerical model. PhD Dissertation, Center for Computational Hydroscience and Engineering, University of Mississippi, University, Mississippi.

Duan, G., Wang, S.S.Y., Jia, Y., 2001. The applications of the enhanced CCHE2D model to study the alluvial channel migration processes. J. Hydraul. Res., IAHR 39, 469–480.

Dunne, T., Leopold, L.B., 1978. Water in Environmental Planning. W.H. Freeman, San Francisco. 818 pp.

Eaton, B.C., Church, M., Millar, R.G., 2004. Rational regime model of alluvial channel morphology and response. Earth Surf. Proc. Land. 29, 511–529.

Engelund, F., 1974. Flow and bed topography in channel bends. J. Hydraul. Div., ASCE 100 (11), 1631–1648.

Ferguson, R.I., 1973. Channel pattern and sediment type. Area 5, 38–41.

Friedkin, J., 1945. A laboratory study of the meandering of alluvial rivers. Technical Report 13, US Waterways Experiment Station, Vicksburg, Mississippi.

Glover, R.E., Florey, Q.L., 1951. Stable channel profiles, vol. 235. US Bureau of Reclamation, Denver, CO.

Hasegawa, K., 1981. Bank–erosion discharge based on a non-equilibrium theory. Proc. JSCE, Tokyo, 316, 37–50 (in Japanese).

Hey, R.D., Thorne, C.R., 1986. Stable channels with mobile gravel beds. J. Hydraul. Eng. Div., ASCE 112, 671–689.

Hickin, E.J., 1972. Pseudomeanders and point dunes—a flume study. Am. J. Sci. 272, 762–799.

Hickin, E.J., 1977. The analysis of river–planform responses to changes in discharge. in River Channel Changes, edited by K.J. Gregory, Wiley, chichester, England, 249–263.

Hickin, E.J., Nanson, G.C., 1975. The character of channel migration on the beatton river, northeast British Columbia, Canada. Geol. Soc. Am. Bull. 86, 487–494.

Hooke, J.M., 1980. Magnitude and distribution of rates of river bank erosion. Earth Surf. Proc. Land. 5, 143–157.

Huang, H.Q., Nanson, G.C., 2000. Hydraulic geometry and maximum flowefficiency as products of the principle of least action. Earth Surf. Proc. Land. 25, 1–16.

Ikeda, S., 1989. In: Ikeda, S., Parker, G. (Eds.), Sediment Transport and Sorting at Bends in Flow in Meandering Channels. American Geophysical Union, pp. 103–125.

Ikeda, S., Izumi, N., 1990. Width and depth of self-formed straight gravel rivers with bank vegetation. Water Resour. Res. 26 (10), 2353–2364.

Ikeda, S., Parker, G., Sawai, K., 1981. Bend theory of river meanders. Part I. Linear development. J. Fluid Mech. 112, 363–377.

Ikeda, S., Parker, G., Kimura, Y., 1988. Stable width and depth of straight gravel rivers with heterogeneous bed materials. Water Resour. Res. 24 (5), 713–722.

Imran, J., Parker, G., Pirmez, C., 1999. A nonlinear model of flow in meandering submarine and subaerial channels. J. Fluid Mech. 400, 295–331.

Johannesson, H., 1985. Computer simulated migration of meandering rivers. MS Thesis, University of Minnesota, Minneapolis, MN, 115p.

Johannesson, H., Parker, G., 1989. Velocity redistribution in meandering rivers. J. Hydraul. Eng. 115 (8), 1019–1039.

Julien, P.Y., 2002. River Mechanics. Cambridge University Press, Cambridge. 434 p.

Kellerhals, R., Church, M., 1989. The morphology of large rivers: characterization and management. In: Dodge, D.P. (Ed.), Proceedings of the International Large River Symposium Special Publication 106, Canadian Journal of Fisheries and Aquatic Sciences, pp. 31–48.

Kikkawa, H., Ikeda, S., Kitagawa, A., 1976. Flow and bed topography in curved open channels. J. Hydraul. Div., ASCE 102 (9), 1327–1342.

Kirkby, M.J., 1977. Maximum sediment efficiency as a criterion for alluvial channels. In: Gregory, K.J. (Ed.), River Channel Changes. Wiley, Chichester, pp. 429–442.

Knighton, D., 1998. Fluvial Forms and Processes. Edward Arnold, London. 400 pp.

Kovacs, A., Parker, G., 1994. A new vectorial bedload formulation and its application to the time evolution of straight river channels. J. Fluid Mech. 267, 153–183.

Lane, E.W., 1955. Design of stable channels. Trans. ASCE 120, 1234–1260.

Langbein, W.B., Leopold, L.B., 1966. River meanders: theory of minimum variance, Professional Paper 422-H. US Geological Survey.

Larsen, E.W., 1995. Mechanics and modeling of river meander migration. PhD Dissertation, University of California, Berkeley, CA.

Leopold, L.B., Maddock, T., 1953. The hydraulic geometry of stream channels and some physiographic implications, Professional Paper, 252. US Geological Survey. 57 pp.

Millar, R.G., Quick, M.C., 1993. Effect of bank stability on geometry of gravel rivers. J. Hydraul. Eng., ASCE 119 (12), 1343–1363.

Millar, R.G., Quick, M.C., 1998. Stable width and depth of gravel-bed rivers with cohesive banks. J. Hydraul. Eng. 124 (10), 1005–1013.

Montgomery, D.R., Gran, K.B., 2001. Downstream variations in the width of bedrock channels. Water Resour. Res. 37 (6), 1841–1846.

Mosselman, E., 1998. Morphological modeling of rivers with erodible banks. Hydrol. Process. 12, 1357–1370.

Nagata, N., Hosoda, T., Muramoto, Y., 2000. Numerical analysis of river channel processes with bank erosion. J. Hydraul. Eng. 126 (4), 243–252.

Nanson, G.C., Hickin, E.J., 1983. Channel migration and incision on the Beatton River. J. Hydraul. Eng. 109, 227–327.

Nelson, J.M., Smith, J.D., 1989. Evolution and stability of erodible channel beds. In: Ikeda, S., Parker, G. (Eds.), River Meandering, pp. 321–377 (AGU).

Odgaard, A.J., 1989. River meander model. I. Development. J. Hydraul. Eng. 115 (11), 1433–1450.

Olsen, N.R.B., 2003. Three-dimensional CFD modeling of self-forming meandering channel. J. Hydraul. Eng. 129 (5), 366–372.

Osman, A.M., Thorne, C.R., 1988. Riverbank stability analysis. 1. Theory. J. Hydraul. Eng., ASCE 114, 134–150.

Parker, G., 1978. Self-formed straight rivers with equilibrium banks and mobile bed. Part 2. The gravel river. J. Fluid Mech. 89 (1), 127–146.

Parker, G., 1983. Theory of meander bend deformation. In: Elliott, C.M. (Ed.), River Meandering Proceedings of ASCE River'83 Conference, ASCE, pp. 722–731.

Parker, G., Andrew, E.D., 1986. On the time development of meander bends. J. Fluid Mech. 162, 139–156.

Parker, G., Sawai, K., Ikeda, S., 1982. Bend theory of river meanders. Part II. Nonlinear deformation of finite-amplitude bends. J. Fluid Mech. 115, 303–314.

Parker, G., Diplas, P., Akiyama, J., 1983. Meander bends of high amplitude. J. Hydraul. Eng. 109 (10), 1323–1337.

Pizzuto, J.E., 1994. Channel adjustments to changing discharges, Powder River, Montana. Geol. Soc. Am. Bull. 106, 1494–1501.

Rosgen, D., 1996. Applied River Morphology. Wildland Hydrology, Pagosa Springs, CO.

Schumm, S.A., 1968. River adjustment to altered hydrologic regime—Murumbidgee River and Paleochannels, Australia, Professional Paper, No.598. US Geological Survey. 65 pp.

Schumm, S.A., 1985. Patterns of alluvial rivers, Ann. Rev. Earth Planet Sci., 13, 5–27.

Schumm, S.A., Mosley, M.P., Weaver, W.E., 1987. Experimental Fluvial Geomorphology. Wiley, New York. 413 pp.

Shiono, K., and Muto, Y., 1998. Complex flow mechanisms in compound meandering channel for overbank flow. *J. Fluid Mech.,* 376, 221–261.

Silva, A., 1995. Turbulent Flow in Sine-generated Meandering Channel. PhD Dissertation, Queen's University, Kingston, Ont., Canada.

Simon, A., Curini, A., Darby, S.E., Langendoen, E.J., 2000. Bank and near-bank processes in an incised channel. Geomorphology 35, 193–217.

Simon, A., and Thorne, C.R., 1996. Channel adjustment of an unstable coarse-grained stream: Opposing trends of boundary and critical shear stress, and the applicability of extremal hypotheses. *Earth Surface Processes and landforms*, 21, 155–180.

Smith, J.D., Mclean, S.R., 1984. A model for flow in meandering streams. Water Resour. Res 20 (9), 1301–1315.

StØlum, H.H., 1998. Planform geometry and dynamics of meandering rivers. GSA Bull. 110 (11), 1485–1498.

Sun, T., Meakin, P., JØssang, T., Schwarz, K., 1996. A simulation model for meandering rivers. Water Resour. Res. 32, 2937–2954.

Sun, T., Meakin, P., JØssang, T., 2001. Meander migration and the lateral tilting of floodplains. Water Resour. Res. 37 (5), 1485–1502.

Sun, T., Meakin, P., JØssang, T., 2001. A computer model for meandering rivers with multiple bed load sediment sizes. I. Theory. Water Resour. Res. 37 (8), 2227–2241.

Vigilar, G.G., Diplas, P., 1997. Stable channels with mobile bed: formulation and numerical solution. J. Hydraul. Eng. 123 (3), 189–199.

White, W.R., Bettess, R., Paris, E., 1982. Analytical approach to river regime. J. Hydraul. Div. 108, 1179–1193.

Williams, G.P., 1978. Hydraulic geometry of river cross sections—theory of minimum variance, Professional Paper, No.1029. US Geological Survey. 47 pp.

Yang, C.T., 1976. Minimum unit stream power and fluvial hydraulics. J. Hydraul. Div. 102, 769–784.

Zimmerman, C., Kennedy, J.F., 1978. Transverse bed slopes in curved alluvial streams. J. Hydraul. Div. 104 (HY1), 33–48.